Published OnlineFirst July 2, 2018; DOI: 10.1158/1541-7786.MCR-18-0212

Signal Transduction

Molecular Cancer Research

Adaptive Resistance to EGFR-Targeted Therapy by Calcium Signaling in NSCLC Cells

Celine Mulder[1], Nadine Prust[1], Sander van Doorn[1], Maria Reinecke[2,3], Bernhard Kuster[2,3], Paul van Bergen en Henegouwen[4], and Simone Lemeer[1]

Abstract

Targeted therapies against oncogenic receptor tyrosine kinases (RTK) show promising results in the clinic. Unfortunately, despite the initial positive response, most patients develop therapeutic resistance. Most research has focused on acquired resistance occurring after an extensive time of treatment; however, the question remains as to how cells can survive an initial treatment, as early resistance to apoptosis will enable cells to develop any growth-stimulating mechanism. Here, the non–small cell lung cancer (NSCLC) PC9 cell line was used to systematically profile, by mass spectrometry, changes in the proteome, kinome, and phosphoproteome during early treatment with the EGFR inhibitor afatinib. Regardless of the response, initial drug-sensitive cells rapidly adapt to targeted therapy, and within days, cells regained the capacity to proliferate, despite persisting target inhibition. These data reveal a rapid reactivation of mTOR and MAPK signaling pathways after initial inhibition and an increase in abundance and activity of cytoskeleton and calcium signaling–related proteins. Pharmacologic inhibition of reactivated pathways resulted in increased afatinib efficacy. However more strikingly, cells that were restricted from accessing extracellular calcium were extremely sensitive to afatinib treatment. These findings were validated using three additional inhibitors tested in four different NSCLC cell lines, and the data clearly indicated a role for Ca^{2+} signaling during the development of adaptive resistance. From a therapeutic point of view, the increased inhibitor efficacy could limit or even prevent further resistance development.

Implications: Combined targeting of calcium signaling and RTKs may limit drug resistance and improve treatment efficacy. *Mol Cancer Res; 16(11); 1773–84. ©2018 AACR.*

Introduction

Constitutively active kinases often drive tumor cell survival and proliferation. Consequently, a multitude of small-molecule inhibitors targeting these kinases have been developed. About 23 tyrosine kinase inhibitors (TKI) have been approved to date, showing promising results in the clinic (1, 2). However, despite an initial positive response, most patients eventually develop resistance against the inhibitor. Long-term, or acquired, resistance has been studied extensively, mainly concentrating on identifying additional mutations that are either acquired or preexisting (3). Simultaneous inhibition of multiple potential resistance mechanisms delays, however, does not prevent development of resistance (4, 5). Therefore, the most challenging question remains how cancer cells adapt to and survive initial inhibitor treatment, enabling them to develop acquired resistance.

Currently, two major hypotheses have been formulated trying to explain the development of resistance (6). First, intrinsically resistant clones may exist through the heterogeneity within the tumor (7). These preexisting clones would be positively selected by targeted treatment. Alternatively, resistance could arise as tumor cells collectively adapt under pressure of drug treatment. This would be similar to antibiotic resistance caused by premature ending of a treatment: incomplete eradication of a tumor could strengthen remaining cancer cells (8). Consequently, resistance can develop when proliferation is inhibited, but cell death is not triggered. Unfortunately, small-molecule inhibitors are mostly cytostatic, in contrast with the more cytotoxic chemotherapies. Nevertheless, they are highly specific and show great promise in clinical studies, and should therefore not be discarded (9). In order to improve efficacy, inhibitors are combined with either chemotherapy, immunotherapy, or another form of targeted therapy. Compared with monotreatment, combinational treatment often improves the patients' response, but unfortunately also increases toxicity (10, 11).

Lung cancer is one of the most prevalent cancer types and has a very high mortality rate in both men and women. Non–small cell lung cancer (NSCLC) makes up approximately 85% of the lung cancer cases (12) and is currently treated by surgery, radiotherapy, chemotherapy, targeted therapy with small-molecule inhibitors, or a combination thereof. EGFR overexpression and mutations are driving the disease in a substantial percentage (estimated more than 60%) of NSCLC patients (13, 14).

[1]Biomolecular Mass Spectrometry and Proteomics, Bijvoet Center for Biomolecular Research and Utrecht Institute for Pharmaceutical Sciences, Utrecht University, Utrecht, the Netherlands. [2]Chair of Proteomics and Bioanalytics, Technical University Munich, Freising, Germany. [3]German Cancer Consortium (DKTK), German Cancer Research Center (DKFZ), Heidelberg, Germany. [4]Division of Cell Biology, Science Faculty, Department of Biology, Utrecht University, Utrecht, the Netherlands.

Note: Supplementary data for this article are available at Molecular Cancer Research Online (http://mcr.aacrjournals.org/).

Corresponding Author: Simone Lemeer, Utrecht University, Padualaan 8, 3584 CH Utrecht, the Netherlands. Phone: 0031-30-253-9974; E-mail: S.M.Lemeer@uu.nl

doi: 10.1158/1541-7786.MCR-18-0212

Published OnlineFirst July 2, 2018; DOI: 10.1158/1541-7786.MCR-18-0212

Here, we set out to identify the initial survival pathways that become activated in NSCLC cells harboring an EGFR-activating mutation, after treatment with the EGFR-specific inhibitor afatinib, and subsequently to inhibit these pathways to increase drug efficacy. By targeting the pathways tumor cells use to adapt and survive drug treatment, the specificity of the small-molecule inhibitor is further exploited: only cells that are responding to the first treatment will be sensitive to the second, preferably cytotoxic, agent. This differs from the standard combination with chemotherapy, which targets all rapidly dividing cells. We used mass spectrometry to elucidate the changes in the proteome, kinome, and phosphoproteome in the NSCLC cell line PC9, induced by the TKI afatinib, which specifically targets EGFR. Here, we show that, upon treatment, NSCLC cells differentially regulate Ca^{2+} signaling and enhance Ca^{2+}-dependent cell adhesion. By limiting the access to extracellular calcium during TKI treatment, we increased growth inhibition and induced apoptosis, decreasing the abilities of the cells to develop acquired resistance. These results were confirmed in multiple combinations of NSCLC cell lines with EGFR-activating mutations and several EGFR inhibitors.

Materials and Methods

Cells and compounds

Inhibitors afatinib, gefitinib, erlotinib, selumetinib, sapanisertib, and rapamycin were purchased from Selleckchem. EGTA and lanthanum(III) Chloride hydrate were purchased from Sigma-Aldrich. Cell lines NCI-H1975, NCI-H1650, and HCC827 were derived from the ATCC, and PC9 was derived from Sigma. EGFR-pTyr1068, Paxillin-pTyr31, and Actin antibodies were from Abcam. EGFR, Myosin-IIa, Myosin-IIa-pSer1943, Myosin-IIc, Erk1/2, ERK1/2-pThr208/pTyr206, RPS6, RPS6-p-Ser235/Ser236, MAPK14, Paxillin, Paxillin-pTyr118, FAK, FAK-pTyr576/577, and FAK-pTyr397 antibodies were from Cell Signaling Technology. GAPDH was derived from GeneTex.

IncuCyte, scratch assay, apoptosis, and IC_{50} curves

Cells were plated 1,500 cells (PC9/H1975) or 2,500 (H1650/HCC827) per 96-well. An IncuCyte System (Essen Bioscience) was used to monitor cell growth. For the wound scratch assay, scratches were made using the IncuCyte wound maker. Apoptosis was measured using the IncuCyte Caspase-3/7 Apoptosis Assay (Essen Bioscience), according to the manufacturer's protocol. Viability was measured using AlamarBlue Cell Viability Assay (Thermo Fisher Scientific), and IC_{50} curves were fitted using a nonlinear fit curve fitting in GraphPad Prism 7.

Western blot

A total of 20 to 30 μg cell lysates were run on a precast gel (Bio-Rad, 12% SDS). Proteins were transferred to a PVDF membrane in transfer buffer [1x TG buffer (Bio-Rad), 20% methanol]. Membranes were blocked with 5% milk or BSA before incubation with primary antibody overnight at 4°C. Membranes were incubated with secondary antibodies (Dako) for 2 hours at room temperature, and bands were made visible by Pierce ECL Plus Substrate (Thermo).

Cell culture

Cells were cultured in a humidified atmosphere and 5% CO_2. Growth medium was RPMI 1640 medium (Lonza), supplemented with 10% FBS (Thermo), 1% Pen/Strep (Lonza), and L-glutamine (Lonza). Cells were tested negative for mycoplasma infections on a regular basis.

For proteomics, proteins were labeled with heavy amino acids Arginine-6 and Lysine-4 in DMEM depleted of light amino acids (Buchem BV). Cells were cultured for a minimum of 5 passages to achieve complete labeling.

Cell lysis and digestion

Before lysis, all cells were washed with cooled PBS (Lonza). For proteome analysis, cells were lysed in 1% SDC, 10 mmol/L TCEP, 100 mmol/L TRIS, and 40 mmol/L chloroacetamide (Sigma); protease inhibitors (Complete mini tablet, EDTA-free, Roche); and phosphatase inhibitors (PhosSTOP tablet, Roche). Next, lysates were sonicated (15 cycles, 30 seconds on, 30 seconds off). For Phosphoproteomics, cell pellets were lysed in 7 mol/L urea, 1% triton, 100 mmol/L TRIS, 5 mmol/L TCEP, 30 mmol/L CAA, 10 units/mL DNAse1, 1 mmol/L Pervanadate, 1% Benzonase, 2.5 mmol/L Mg^{2+}, phosphatase inhibitor, and protease inhibitors. Next, proteins were precipitated using methanol/chloroform precipitation. Proteins were overnight digested with Trypsin (Sigma). Peptides were desalted using Seppack C18 column [1cc (50 mg), Waters Corp.].

For Kinobead analysis, cells were lysed in lysis buffer containing 50 mmol/L TRIS, 5% glycerol, 1.5 mmol/L $MgCl_2$, 150 mmol/L NaCl, 1 mmol/L Na_3VO_4, 25 mmol/L NaF, 0.8% NP40, protease inhibitors, and cocktail of phosphatase inhibitors (see for details, Supplementary Materials and Methods).

High-pH fractionation, Fe^{3+}-IMAC, kinobead analysis before LC-MS/MS analysis

For proteome analysis, 100 μg desalted cell lysate was fractionated on a high-pH gradient. Peptides were loaded in buffer A (10 mmol/L NH_4OH, pH 10) on a Phenomenex Gemini C18 3 μm 100 × 1.0 mm column using an Agilent 1200 HPLC system. A gradient of buffer B (10 mmol/L NH_4OH in 90% ACN, pH 10) was used for elution. Fractions were analyzed separately (51).

For phosphopeptide enrichment, peptides were loaded on a Fe^{3+}-IMAC column (Propac IMAC-10 4 × 50 mm column; Thermo; ref. 16). After wash with buffer A (30% ACN, 0.07% TFA), peptides were eluted with a gradient of buffer B (0.3% NH_4OH). Using a UV-abs signal, the outlet of the column was monitored, and one phospho fraction was collected. Phosphorylated peptides were dried in a speedvac and stored at –80°C.

For kinobead analysis, 2 mg of cell lysate was enriched for kinases in a 96-well format using the kinobead assay as described previously (15). After enrichment, the eluates were digested using in-gel digestion.

Subsequently, peptides were analyzed on an Agilent 1290 LC system (Agilent Technologies) coupled to an Orbitrap Q-Exactive HF (Thermo).

Data analysis

RAW files were searched with MaxQuant. Further data processing was done using Perseus (v. 1.5.0.0), TIBCO Spotfire (v. 7.6.0.39), Metascape Excel Add-In (v 1.0.0.10), and PHOTON (17). *P* value of ratios were calculated per time point using the Student unequal variance *t* test for all datasets. In addition for proteomics and phosphoproteomics data an ANOVA, *P* value was calculated. Significance was determined by correcting the *P* value for multiple testing using an FDR of 5% (S0 set to 1, 250 randomizations).

Published OnlineFirst July 2, 2018; DOI: 10.1158/1541-7786.MCR-18-0212

Supplementary Materials and Methods

Additional information on used methods is provided in the Supplementary information.

ProteomeXchange accession

The mass spectrometry proteomics data have been deposited to the ProteomeXchange Consortium via the PRIDE partner repository with the dataset identifier PXD008454.

Results

PC9 cells showed a clear but incomplete response to TKI treatment

With the aim of performing a multi-omic analysis of initial drug resistance, we first characterized the cellular response to small-molecule inhibitor treatment. The NSCLC cell line PC9, which harbors an activating deletion in the EGFR (DelE746A750), was highly sensitive to treatment with first- (gefitinib, erlotinib) and second-generation (afatinib) EGFR inhibitors, as shown by the measurement of viability after 3 days of treatment (Fig. 1A). However, despite the pronounced effect, around 30% of viability persisted. In order to better characterize the properties of the persisting cells, we analyzed various hallmarks of cancer, including proliferation, apoptosis, and migration. Proliferation analysis showed that untreated cells grew to full confluence within 3 days, where cells treated with 10 nmol/L, 100 nmol/L, or 1 μmol/L afatinib, or 1 μmol/L erlotinib or gefitinib, needed 6 to 7 days (Fig. 1B). Although the proliferation rate of treated cells decreased, cells were still able to grow to full confluence despite the continuous inhibition of

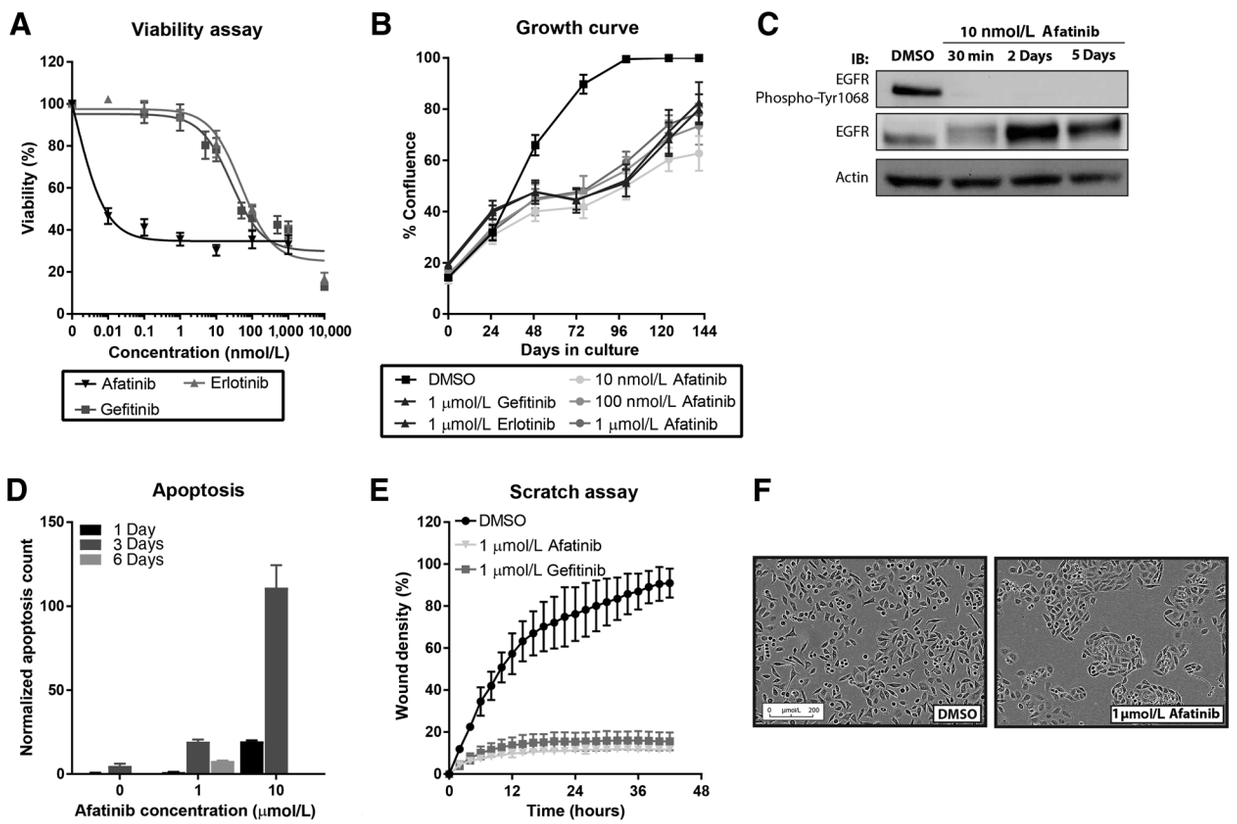

Figure 1.

Phenotyping PC9 NSCLC cells upon TKI treatment. **A,** To determine drug response, PC9 cells were treated with different concentrations of three inhibitors (afatinib, gefitinib, and erlotinib) for 3 days. Viability was measured using AlamarBlue. Relative viability of cells treated with inhibitors as compared with untreated cells is plotted on the *Y* axis. Error bars represent 4 replicate wells within one experiment. **B,** Growth curves of PC9 cells showed incomplete growth inhibition upon EGFR inhibition, independent of the type of inhibitor or concentration. Confluence of cells treated with 10 nmol/L, 100 nmol/L, or 1 μmol/L TKI was monitored using the IncuCyte System over a time span of 6 days. Error bars represent quadruple wells within one experiment. Medium in the wells was refreshed every 3 days. **C,** Western blot of PC9 cells treated with DMSO or 10 nmol/L afatinib for 30 minutes, 2 days, or 5 days showed clear inhibition of EGFR activity during our experiments. Antibodies were used against the EGFR protein to show protein expression and against EGFR phosphorylated on Tyr1068 as indication of activity. Actin was used as a loading control. **D,** To monitor apoptosis during EGFR inhibition, PC9 cells were treated with 1 μmol/L afatinib for 1, 3, or 6 days. Upon treatment, only minor amounts of apoptosis were observed, as compared with a negative control (DMSO) and a positive control (10 μmol/L afatinib, cytotoxic concentration). Both negative and positive controls were discontinued after 3 days. Error bars represent quadruple replicate wells of which four images were taken as technical replicates. Apoptosis was measured using the Caspase 3/7 green fluorescent probe using the IncuCyte System. Fluorescent count was normalized on well confluence per image. **E,** In order to quantify migration, confluent PC9 cells were treated with DMSO or 1 μmol/L afatinib or gefitinib for up to 48 hours. At the beginning of this treatment, a scratch was made in each 96-well, and confluence within the scratch was measured using the IncuCyte System. Error bars represent four replicate scratches. **F,** Representative light microscopy pictures of PC9 cells treated with DMSO or 1 μmol/L afatinib for 3 days to show clear morphologic changes upon treatment.

Published OnlineFirst July 2, 2018; DOI: 10.1158/1541-7786.MCR-18-0212

the primary drug target, as shown by the decreased levels of EGFR-Y1068 phosphorylation (Fig. 1C).

For apoptosis measurements, cells were treated with DMSO (negative control) or 1 or 10 μmol/L afatinib (cytotoxic concentration as positive control). Untreated cells grew to full confluence, whereas 10 μmol/L afatinib-treated cells showed 100% apoptosis, and consequently, measurements were discontinued for these conditions after 3 days (Supplementary Fig. S1A). Cells treated with 1 μmol/L afatinib showed a significant increase in levels of apoptosis compared with untreated cells (Fig. 1D). However, when compared with the positive control, only one fifth of the response was detected, indicating that the majority of the cells did not go in apoptosis. More surprisingly, after 6 days of afatinib treatment, levels of apoptosis decreased again (Fig. 1D). Finally, complete abolishment of migration after treatment was shown by a scratch assay (Fig. 1E; Supplementary Fig. S1B). This lack of migration caused formation of tight clusters of cells (Fig. 1F; Supplementary Videos). Collectively, these results show a clear response by PC9 cells upon afatinib treatment: it abolished migration and induced both growth inhibition and a small amount of apoptosis. However, a majority of cells persisted. After only 3 days, these cells were increasingly resistant to apoptosis and continued to grow despite the continuous inhibition of the EGFR.

Mass spectrometry–based multi-omic profiling of afatinib response

In order to detect the changes that would be responsible for continued growth in the presence of the drug, PC9 cells were treated with afatinib for 1 to 7 days at a concentration of 10 nmol/L, and the proteome, phosphoproteome, and kinome were analyzed at various time points (1–7 days). The selected concentration represents 10x the concentration at which we start to observe the stable presence of viable cells (Fig. 1A). After treatment, proteins were fractionated using high-pH chromatography for full proteome analysis (Supplementary Table S1). Principle component analysis (PCA) showed clustering of replicates and a clear separation of time points, indicating changes on proteome level over time (Supplementary Fig. S2A). An additional kinobead pulldown was used to detect expression changes on kinome level (Supplementary Table S2; ref. 15). As shown by the PCA plot, most variation exists between DMSO of 24 to 48 hours and 72 hours to 7 days, whereas less difference exists within these two groups (Supplementary Fig. S2B).

To detect changes at the signaling level, phosphopeptides were enriched using a Fe^{3+}-IMAC column (16). Cells were treated with 10 nmol/L afatinib for 30 minutes to determine immediate drug effects, and for 2 and 5 days to detect long-term changes (Supplementary Table S3). A PCA plot of all identified peptides showed a clear separation between untreated and 30 minutes, versus 2 and 5 days of treatment (Supplementary Fig. S2C). The collective dataset (Supplementary Tables S1, S2, and S3) comprises quantitative information for >5,600 proteins, >270 protein kinases, and >22,900 phosphopeptides (>18,400 unique phosphorylation sites).

An ANOVA test was performed to detect all differentially regulated proteins between time points (Fig. 2A). Up- and down-regulated proteins were analyzed for GO terms, showing decreased translation and mRNA processing, and increased actin cytoskeleton construction and calmodulin binding.

Hierarchical clustering of phosphoproteome data shows in total 2,483 regulated phosphosites with a P value of <0.05 according to an ANOVA test, in at least one time point versus DMSO (Fig. 2B). In order to include reactivated phosphosites, regulated sites between 2/5 days and 30 minutes were also included in the clustering. Based on the clustering, we selected four clusters on which GO term analysis was performed. Interestingly, all clusters showed enrichment for adhesion and cytoskeleton reorganization-related pathways, which is in correlation with the proteome analysis. The two clusters showing regulation between 30 minutes and 2 to5 days of treatment were additionally enriched for cell-cycle–related pathways.

Unlike proteomics data, the direction of regulation of a phosphopeptide is not always indicative of the direction of the activity of the protein: phosphorylation can either inhibit or activate the protein. Because functional consequences of phosphorylation are often not known, it can be difficult to define changes of functionality based only on measured ratios. To solve this problem, we transformed peptide level ratios into functionality scores on the protein level using the tool PHOTON (17). Hierarchical clustering of PHOTON scores indicated that most of the activated sites were enriched for Ca^{2+}-related signaling (Fig. 2C). As expected, cell-cycle–related pathways showed decreased activity, confirming that afatinib induced growth inhibition. The cluster showing a decrease after 30 minutes, but an increase after 2 and 5 days, was enriched for ErbB signaling. This implies that initially the ErbB pathway is effectively inhibited, but seems to regain activity in time, despite the effective inhibition of EGFR (Fig. 1C).

Reactivated pathways downstream of EGFR

As our phosphoproteomic data indicate, growth-activating pathways downstream of EGFR are reactivated within days. Prominent reactivation of PI3K/mTOR signaling after initial inhibition was observed, for example, indicated by recovery of activity-determining S235/236 phosphorylation in RPS6, a major downstream target of mTOR (Fig. 3A). Western blot analysis of RPS6 phosphorylation confirmed its recovery, whereas RPS6 levels remained constant (Fig. 3B). In addition, MEK/ERK signaling recovered rapidly, as indicated by regained ERK1/2 phosphorylation of the activity-determining sites (Fig. 3A) but unchanged protein expression, which was again confirmed by Western blot analysis (Fig. 3B). Reactivation of both pathways has previously been shown to occur after acquired EGFR inhibitor resistance in a subset of clones (4, 5, 18). In order to test whether this reprogrammed signaling could pharmacologically be exploited, we performed combination treatments with the mTOR inhibitors rapamycin (mTORC1) and sapanisertib (mTORC1/2) and the MEK inhibitor selumetinib. As shown in Fig. 3C, combining rapamycin with afatinib significantly decreased the growth capabilities of the cells compared with afatinib treatment alone, but it did not increase the amount of apoptosis. Treatment with rapamycin alone did affect neither cell viability nor apoptosis. Because rapamycin is solely inhibiting mTORC1, we included the pan mTOR inhibitor sapanisertib (or INK128) in our analysis. Sapanisertib in combination with afatinib did not increase apoptosis and showed similar growth inhibition when compared with afatinib/rapamycin combination treatment. These results indicate that mTORC2 signaling does not contribute to reactivated mTOR signaling after afatinib treatment. In addition, these results indicate that combined mTORC1/afatinib inhibition mainly induces cytostatic effects, and consequently, the development of further resistance pathways cannot be excluded. Combination of the MEK

Published OnlineFirst July 2, 2018; DOI: 10.1158/1541-7786.MCR-18-0212

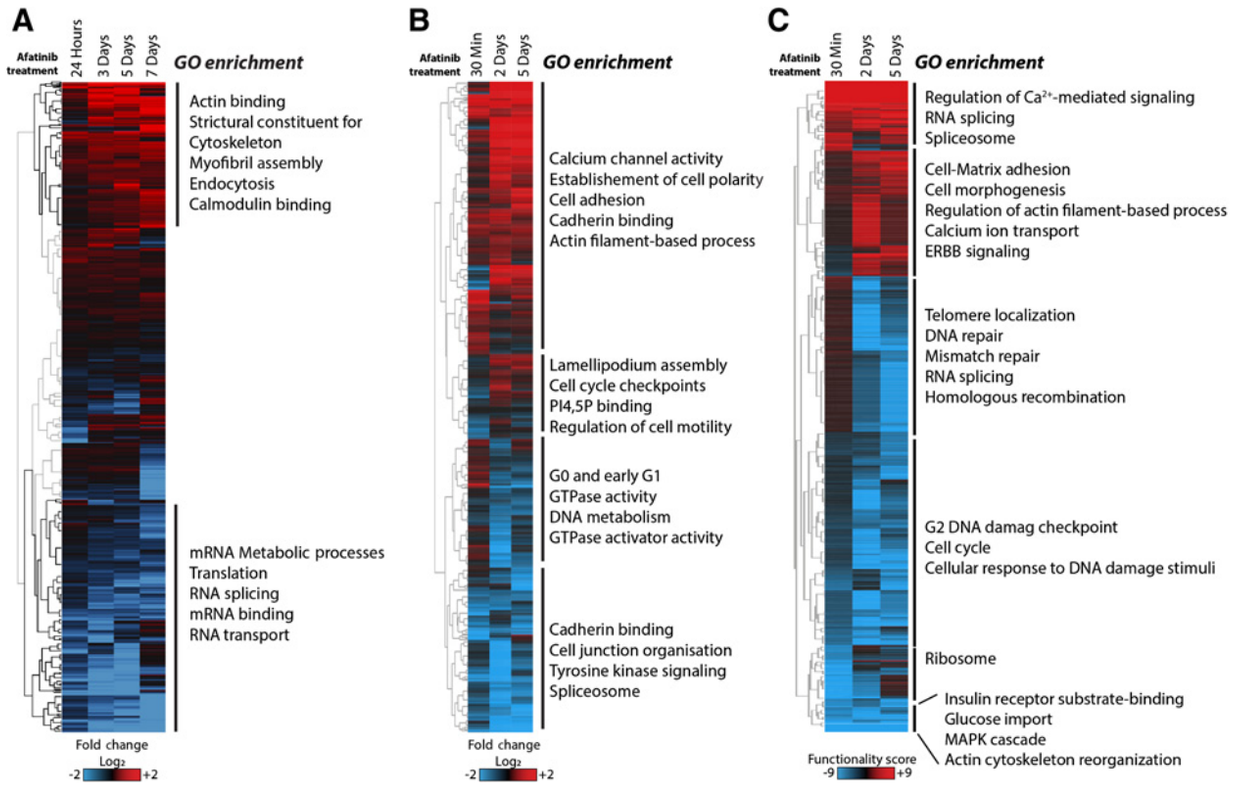

Figure 2.

(Phospho) Proteomics profiling of PC9 cells upon afatinib treatment. **A,** Summarized proteome response of PC9 cells treated with 10 nmol/L afatinib for 1, 3, 5, or 7 days. Hierarchical clustering of the $\log_2$ ratios of the proteins that were significantly distinguished by an ANOVA test between the time points is shown. GO term enrichment analysis, as depicted on the right, demonstrated upregulation of actin-binding processes and downregulation of mRNA and translation-related processes. **B,** Phosphoproteome data of PC9 cells after afatinib treatment showed regulation of cell adhesion, cell cycle, and spliceosome-related processes. PC9 cells were treated with 10 nmol/L afatinib for 30 minutes, 2, and 3 days. All phosphosites that were differentially regulated in at least one time point, as compared with untreated cells or compared with 30 minutes, were shown in a hierarchical clustering. Different clusters were analyzed for GO term enrichment, as depicted on the right. **C,** Phosphoproteome data were reanalyzed using PHOTON, resulting in functionality scores. All phosphoproteins significantly changing in at least one time point were shown in a hierarchical clustering. Different clusters, based on the hierarchical clustering, were analyzed for enriched GO terms, as denoted on the right. In addition to the recurring regulation of adhesion and cell-cycle signaling, calcium signaling was enriched within the activated phosphoproteins.

inhibitor selumetinib with afatinib also resulted in a prominent reduction of cell growth capabilities. However, in contrast to mTOR inhibition and in agreement to what has been shown previously (5), MEK inhibition had a tremendous impact on the amount of apoptosis induced, indicating that such treatment could be beneficial for the eradication of tumor cells (Fig. 3C).

To find the upstream kinases that could be responsible for reactivation of mTOR or ERK1/2, we further scrutinized our data. A well-known acquired resistance mechanism after TKI treatment is the upregulation of different (receptor) tyrosine kinases (19, 20) that would refuel growth-inducing signaling. However, in our (phospho)proteome analysis, we find no obvious indications that this would be the case. Also, the kinobead data did not provide evidence that another tyrosine kinases take over EGFR function (Supplementary Table S2). In the kinobead data, EGFR levels significantly decreased at all time points (Supplementary Fig. S2D; Fig. 4A). This was in contrast to the full proteome analysis (Fig. 4B) and Western blot analysis (Fig. 1C). This discrepancy can be explained by the fact that afatinib irreversibly binds EGFR, which makes EGFR no longer accessible for binding to the kinobeads. This again strongly indicated the continuous presence of the drug and inhibition of the receptor during the course of our experiments.

Ca^{2+} signaling and cytoskeleton organizing–related proteins were highly affected by treatment

As previously discussed, we detected strong reactivation of PI3K/mTOR and ERK pathways, but could not identify an obvious upstream kinase that would be responsible. However, we noticed a large number of regulated (phospho)proteins to be involved in the reorganization of the actin cytoskeleton and Ca^{2+}/Calmodulin-related signaling (Fig. 2). For example, the protein levels of Ca^{2+}-dependent protease Calpain-2 (CAPN2) significantly decreased after afatinib treatment (Fig. 4B). This important protease is responsible for degradation of focal adhesions and Ca^{2+} pumps (21, 22). In line with this, we found the calcium-transporting ATPases, ATP2B4 and ATP2C1, to be significantly upregulated. In addition, the actin cross-linking proteins MARCKS, MARCKSL1, and Calponin-2 (CNN2) were significantly upregulated after treatment. These are proteins that bind actin, resulting in more stiffness and increased adhesion (23, 24). Spectrin super family members, like α-Actinin, SPTAN1, and

Published OnlineFirst July 2, 2018; DOI: 10.1158/1541-7786.MCR-18-0212

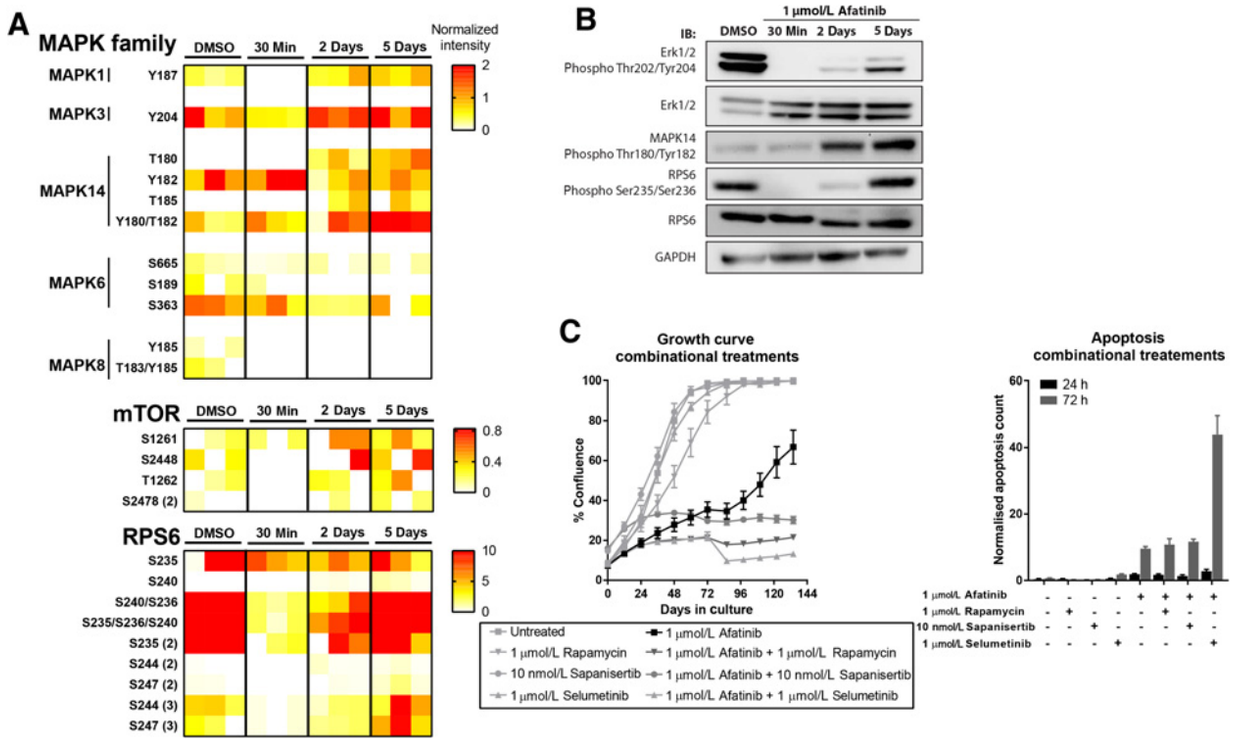

Figure 3.

Proliferation-stimulating pathways are reactivated within days after initial inhibition. **A,** MS data of specified phosphoproteins showed reactivation of activity-determining sites in proteins involved in proliferation-stimulating pathways, including ERK1/2, mTOR, and RPS6. For each individual heatmap, each column represents a replicate of the specified time point and each row an individual phosphopeptide. If a row is annotated with more than one site, or a number in brackets is shown, the peptide was singly, doubly, or triply phosphorylated. Peptides with no multiplicity shown are singly phosphorylated. The color is indicative of the normalized intensity. For this, each protein or protein family has his own legend, due to dynamic range differences. **B,** Validation of MS data on Western blot showed similar patterns of reactivated phosphosites. PC9 cells were treated with 1 µmol/L afatinib for 30 minutes, 2, and 5 days. Antibodies were used against ERK1/2, ERK1/2 phosphorylated on Thr202 and Thr204 respectively, MAPK14 doubly phosphorylated on Thr180 and Thr182, and RPS6 and RPS6 doubly phosphorylated on Ser235 and Ser236. GAPDH was used as a loading control. **C,** MEK and mTOR reactivation was validated by monitoring growth and apoptosis during combinational treatment of EGFR inhibition combined with mTOR (rapamycin: mTOR1; sapanisertib: mTOR1/2) or MEK (selumetinib). Growth was monitored in the IncuCyte System (left). Error bars represent triplicate replicate wells within one experiment. Apoptosis was measured using the Caspase 3/7 Fluorescent probe (right). Fluorescent count was normalized on well confluence per image. Error bars represent triplicate replicate wells of which four images were taken as technical replicates. In both combinations, growth inhibition was increased; however, only the combination of EGFR + MEK inhibition resulted in increased levels of apoptosis.

SPTBN1 that can connect different components of the cytoskeleton, were also upregulated (24).

Levels of EphA4 increased (Fig. 4A; Supplementary Fig. S2D), which has been associated with cytoskeleton rearrangements, inhibiting migration and invasion in NSCLC cell lines and increasing survival in lung cancer patients (25, 26). In contrast, levels of EphA2, a known marker of TKI resistance and stimulator of migration, decreased (27). The levels of Fyn and SIK1 increased over the course of 7 days. Fyn is an Src family kinase, targeting to adherence junctions and a key player in the apoptosis resistance of tumor cells (28). The tumor-suppressing kinase SIK1 phosphorylates and thereby stabilizes p53 to initiate anoikis in case of decreased adhesion (29).

Also, the phosphoproteome data showed regulation of pathways related to Ca^{2+} signaling and actin cytoskeleton organization. After afatinib treatment, two phosphosites of Focal Adhesion Kinase (FAK), the main kinase in the organization of focal adhesions, were found to be downregulated in the phospho data: Ser910 and Ser843, whereas protein levels remained constant (Fig. 5A; Supplementary Tables S1 and S3). Decreased phosphorylation of Ser910 has been shown to reduce proliferation (30). Phosphorylation of Ser843 has been shown to increase upon cellular detachment, implying that the decreased phosphorylation after afatinib treatment is following from increased adhesion (31). In addition, loss of both Ser910 and Ser834 phosphorylation changes cellular morphology and abolishes migration. Tyrosine phosphorylation is, due to relative low abundance, underrepresented in our phosphoproteomics data. Therefore, in order to complement the hypothesis that afatinib treatment is influencing focal adhesion dynamics, some tyrosine phosphorylation sites with established biological functions were analyzed by Western blot (Fig. 5B; ref. 32). Indeed, Tyr397 and Tyr576/577 of FAK as well as Tyr31 and Tyr118 of Paxillin, sites known to stabilize focal adhesions, showed an increase in phosphorylation upon afatinib treatment (Fig. 5B).

The phosphorylation status of Ca^{2+}-binding protein Caldesmon has been linked to its relocation to the cytoskeleton and function to stabilize actin and increased motility (33, 34). As shown by the proteomics data, the protein abundance of

Published OnlineFirst July 2, 2018; DOI: 10.1158/1541-7786.MCR-18-0212

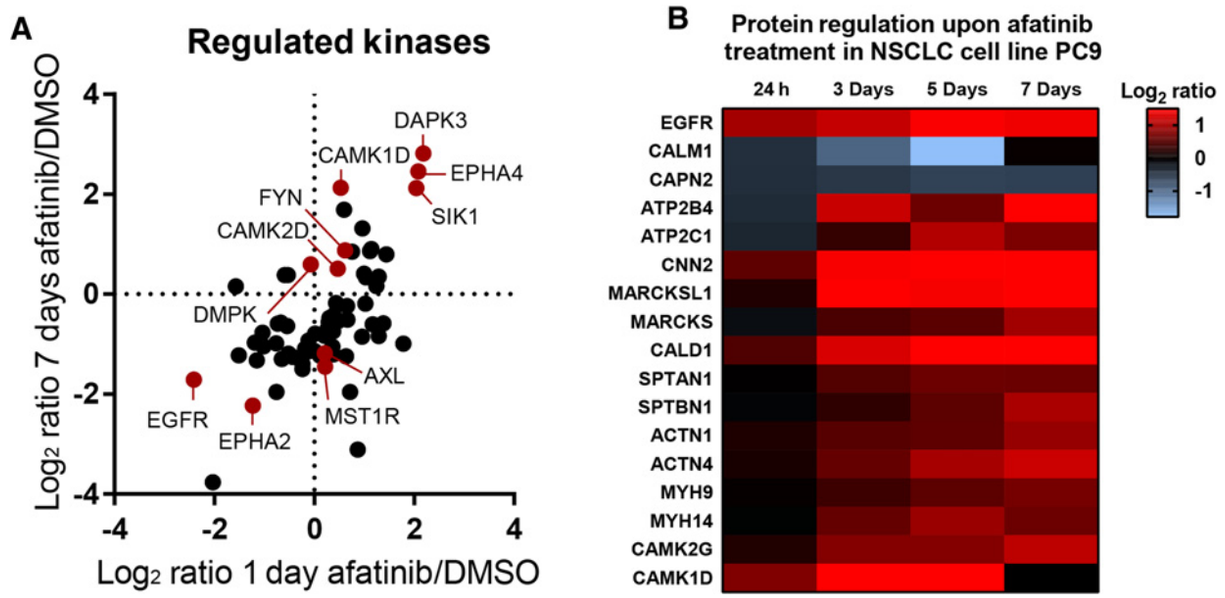

Figure 4.

Regulation of adhesion-related proteins in kinobead and proteomic data. **A,** Upon afatinib treatment, several adhesion-related kinases were differentially regulated, as measured by the kinobead assay. On the *X* axis, the $\log_2$ ratio after 24 hours of afatinib treatment is plotted, on the *Y* axis, the $\log_2$ ratio after 7 days of treatment. Highlighted in red are proteins of interest, labeled with their protein name. **B,** Similarly, in the proteomics data, several adhesion-related proteins were regulated. Log_2 ratios are shown for proteins of interest from the full proteome dataset. Color coding is based on the mean of the three replicate MS runs.

Caldesmon increased upon afatinib treatment (Fig. 4B). In addition, phosphorylation of Caldesmon increased (Fig. 5A). The most severely changing site, Ser789, has been shown to be phosphorylated by ERK1/2 (35). A possible kinase of Caldesmon, CDK14, increased in our kinobead data (Supplementary Fig. S2D).

In nonmuscle cells, three genes comply the myosin protein complex: myosin 9, 10, and 14 (33). Upon phosphorylation, myosins are stabilized, causing increased tension and regulating cell shape, cell polarity, and migration by forming actin-binding filaments. Afatinib treatment increased phosphorylation of myosin (Fig. 5), confirming increased levels on a protein level (Fig. 4B, Fig. 5B). Possible kinases of myosin, the DAPK family, were increasingly phosphorylated and therefore activated (Fig. 5A). DAPKs can be phosphorylated by CAMKs, which increased in both abundance (Fig. 4B; Supplementary Fig. S2B) and phosphorylation (Fig. 5A). Another stimulator of myosin phosphorylation is DMPK, via phosphorylating and inhibiting myosin phosphatase MYPT1 (36). Phosphorylation of MYPT1 on the inhibitory site Thr696 by DMPK was significantly increased after 2 and 5 days of TKI treatment (Fig. 5A).

Depletion of extracellular Ca^{2+} increases sensitivity to TKI treatment

Signaling resulting from increased adhesion has previously been shown to be antiapoptotic (37, 38), and adhesion pathways are largely regulated by Ca^{2+} signaling (39). PC9 cells treated with different TKIs completely abolished migration and formed tight clusters, while resisting apoptosis (Fig. 1). Consistent with this, proteomic analysis showed regulation of both adhesion-related proteins and of Ca^{2+} signaling. Therefore, we hypothesized that the cells use increased adhesion induced by altered Ca^{2+} signaling to resist apoptosis in response to early EGFR inhibition, and that making extracellular calcium unavailable to the cells could inhibit this adhesion and induce apoptosis.

Therefore, we treated PC9 cells with different EGFR inhibitors in the presence or absence of either EGTA, a specific chelator of Ca^{2+} to remove extracellular Ca^{2+}, or Lanthanum(III) Chloride ($LaCl_3$) to block Ca^{2+} uptake. To find a wide applicability, we included the first-generation EGFR inhibitors erlotinib and gefitinib, in addition to afatinib, in our analysis. Treatment with EGTA or $LaCl_3$ alone did not induce any growth defects nor apoptosis in PC9 cells (Fig. 6A). Cells treated with the TKI alone grew in 6 days from 20% to 90% confluence. However, in combination with EGTA or $LaCl_3$ treatment, cells grew in 6 days from 20% to less than 40% confluence, showing increased proliferation inhibition by the addition of EGTA or $LaCl_3$ (Fig. 6A, left). In addition, levels of apoptosis were significantly higher in the presence of EGTA or $LaCl_3$ (Fig. 6A, right). Effects were comparable between the three different inhibitors used, indicating that the development of a Ca^{2+} dependency is not drug specific, but rather EGFR inhibition specific.

To determine whether the observed effect was cell line specific, we tested an additional 3 NSCLC cell lines with different genetic backgrounds and different sensitivities toward the TKIs used (Supplementary Fig. S3A). HCC827 has the exon19del E746-A750 deletion and is highly sensitive to both first (erlotinib and gefitinib) and second (afatinib) generation TKIs. H1975 has both the L858R and the T790M mutation, making it resistant to first, but sensitive to second-generation TKIs. H1650 has the exon19del E746-A750 deletion in combination with PTEN loss, resulting in resistance to first-generation TKIs and a response to treatment with afatinib only upon 1 μmol/L and higher. In all cell lines, neither growth nor apoptosis rate was affected by EGTA

Published OnlineFirst July 2, 2018; DOI: 10.1158/1541-7786.MCR-18-0212

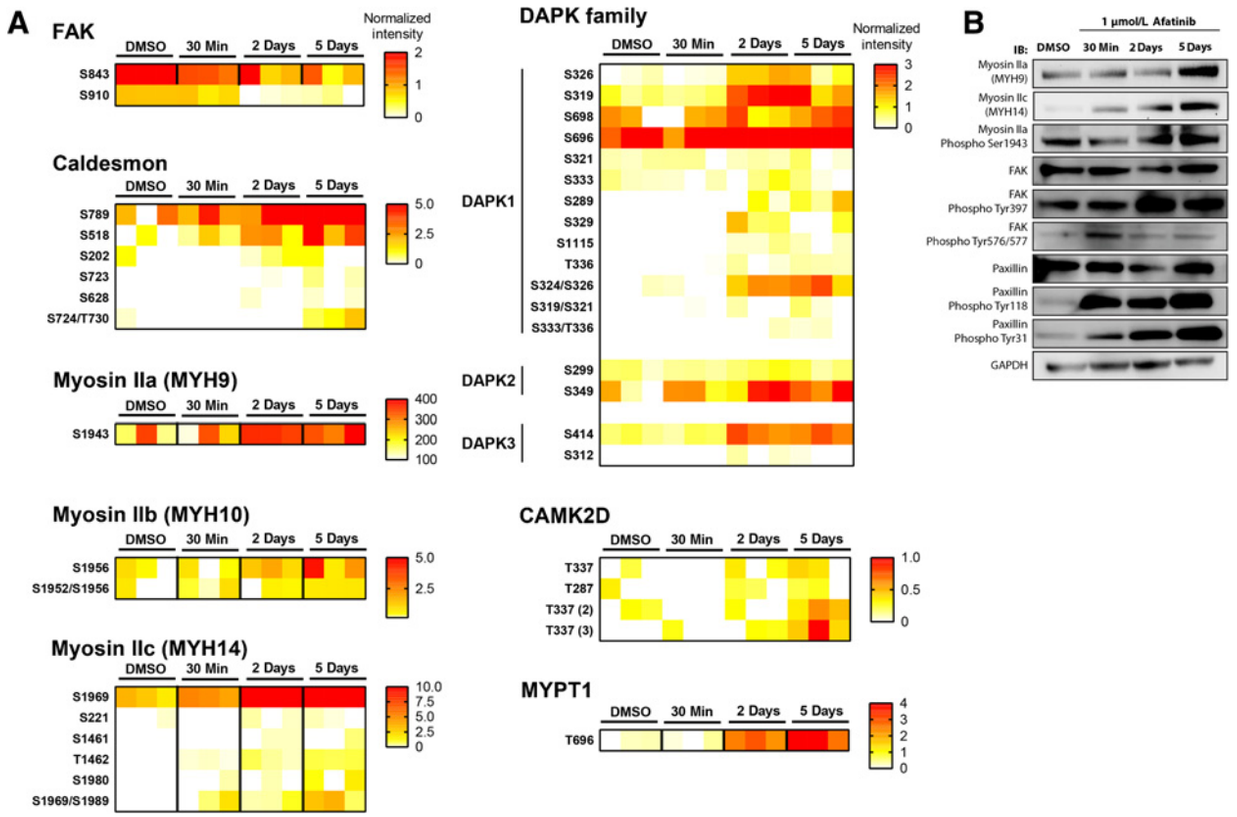

Figure 5.

Phosphoproteomics MS data showed regulated Ca^{2+} signaling. **A,** Regulation of phospho profiles is shown in detail for several proteins of interest. Each column represents a replicate of the specified time point. Each row represents a phosphopeptide. If a row is annotated with more than one site, or a number in brackets is shown, the peptide was singly, doubly, or triply phosphorylated. Peptides with no multiplicity shown are singly phosphorylated. The color is indicative of normalized intensity. For this, each protein or protein family has his own legend, due to dynamic range differences. **B,** Western blot of PC9 cells treated with 1 µmol/L afatinib for 30 minutes, 2, or 5 days showed increased levels of phosphorylation of Myosin IIa and of protein levels of Myosin IIa and IIc. In addition, the Western blot analysis shows increase tyrosine phosphorylation of FAK Tyr397 and Tyr576/577 and Paxillin Tyr31 and Tyr118. GAPDH was used as a loading control.

treatment alone up to 1 mmol/L (Fig. 6B; Supplementary Fig. S3B). However, both the magnitude of the growth inhibition and the amount of apoptosis significantly increased after interference with Ca^{2+} signaling by EGTA or $LaCl_3$ during EGFR inhibition (Fig. 6B). Interestingly, in all cases, apoptosis within the first 24 hours was negligible, but rose significantly in the following 2 to 3 days.

The effect of the combinational treatment was comparable between first- and second-generation TKIs. In contrast, however, the degree of the added effect differed between cell lines, demonstrating high correlation with the sensitivity to the drug (Fig. 6C). HCC827 cell line, which was the most sensitive, displayed the largest added effect of addition of EGTA. H1650 was the most resistant to TKI treatment, showing the lowest increase in levels of apoptosis and growth inhibition after addition of EGTA. In general, the more sensitive a cell line was to TKI treatment, the more sensitive it was for addition of EGTA.

Discussion

Although targeted approaches in cancer therapy show great promise over conventional chemotherapy, development of resistance remains an important obstacle to overcome (9). The majority of resistance studies have focused on acquired resistance mechanisms that occur after an extensive period of treatment, usually by screening for additional mutations. Only recently, attention has shifted to early, adaptive resistance, i.e., why sensitive tumor cells initially survive drug treatment, to subsequently gain additional mutations (8, 40). Here, we hypothesize that rapid adaptation to drug treatment allows incomplete eradication of the tumor, ultimately resulting in additional mutations and a fully resistant tumor. We used a multi-omics approach to elucidate adaptive resistance mechanisms after EGFR-directed TKI treatment with afatinib in NSCLC cells. We demonstrated that NSCLC cells adapt to afatinib inhibition within days and reactivate growth-stimulating pathways, despite continues inhibition of the EGFR. Our data indicate that the cells use altered Ca^{2+} and adhesion signaling as a resistance mechanism, attenuating drug-induced cell death. Interfering with adhesion by Ca^{2+} depletion or limiting access to extracellular Ca^{2+} significantly increased cell death in a TKI-dependent manner.

Our phosphoproteomic data showed that, despite continued inhibition of the EGFR and downregulation of cell-cycle–related pathways, the growth-stimulating mTOR and ERK pathways were

Published OnlineFirst July 2, 2018; DOI: 10.1158/1541-7786.MCR-18-0212

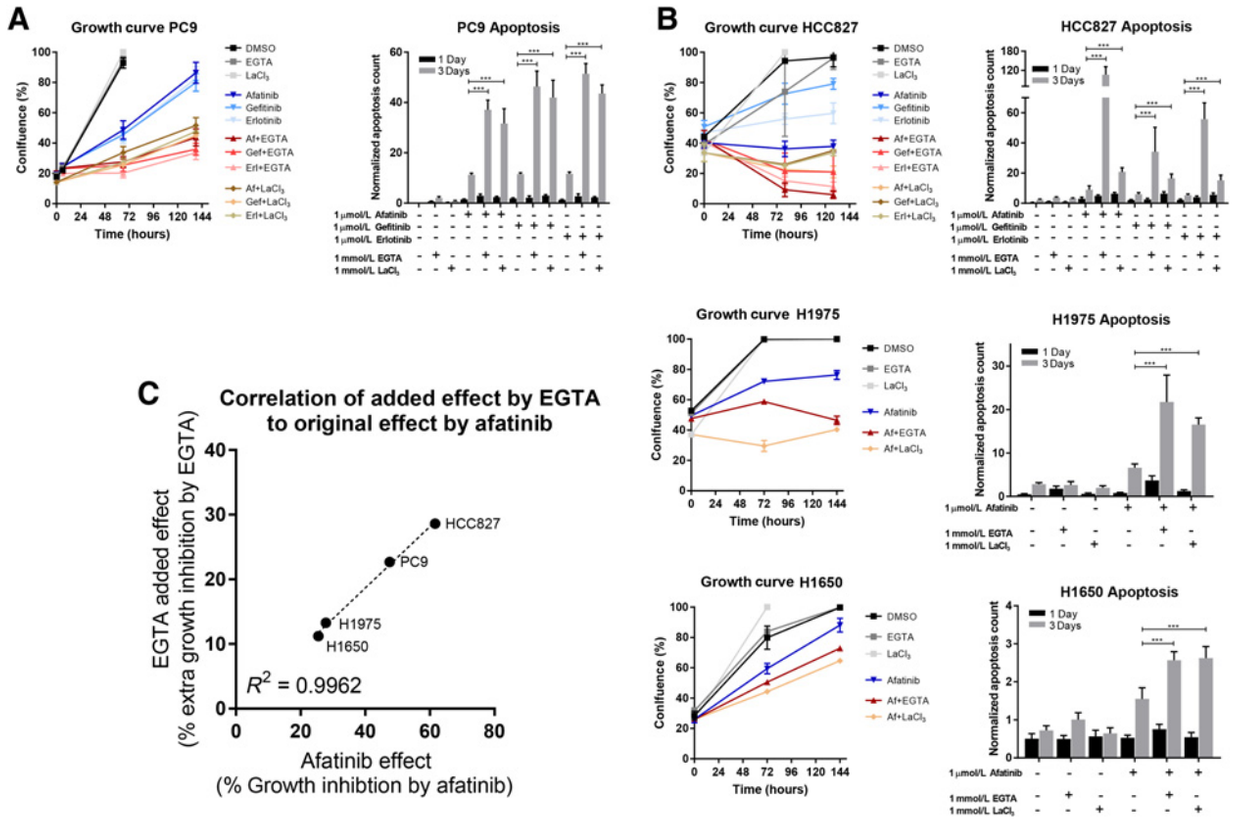

Figure 6.

Ca^{2+} Depletion enhances growth inhibition and induction of apoptosis upon EGFR inhibition. Influence of Ca^{2+} signaling in combination with EGFR inhibition was shown using growth curves and levels of apoptosis. **A,** PC9 cells were grown in the presence or absence of 1 mmol/L EGTA or 1 mmol/L $LaCl_3$, and simultaneously treated with 1 µmol/L EGFR inhibitors (afatinib, gefitinib, or erlotinib). Percentage of confluence was measured to show increased growth inhibition and induction of apoptosis, independent of inhibitor used, as measured with green fluorescent Caspase 3/7 Probe. **B,** Combined EGFR inhibition and interference with Ca^{2+} availability was explored on three different NSCLC cell lines. Confluence and apoptosis were measured in the IncuCyte System. *P* values are depicted above bars: ***, < 0.001. All error bars represent the data of four replicate wells within one experiment. **C,** Growth inhibition induced by afatinib or by afatinib in the presence of EGTA showed great correlation, as shown by a scatter plot. The mean percentage of inhibition after 3 days induced by afatinib is plotted on the *X* axis, where the mean percentage of added effect of EGTA in combination with afatinib was plotted on the *Y* axis. The dotted line indicates the linear regression, and the R^2 is depicted in the graph.

reactivated within days. This correlates with the reactivated growth of NSCLC cells and strongly suggests a rapid adjustment to EGFR inhibition. In agreement with this, pharmacologic inhibition of mTOR and ERK pathways shows a synergistic effect in combination with afatinib treatment. The ERK pathway is most conventionally activated by upstream tyrosine kinase receptors (41). However, ERK kinases can also be activated by several other signaling pathways, for example, integrin signaling via enhanced adhesion (42). Indeed, reactivated growth signaling by increased adhesion is supported by our data in which we find a strong upregulation of adhesion-related proteins after EGFR inhibition. Several regulators of the stability of the cytoskeleton were upregulated upon treatment. In addition, the protease calpain-2, responsible for degradation of focal adhesions, was downregulated. It is intriguing to speculate that increased ERK signaling is induced by increased adhesion via Ca^{2+} signaling as the observed effects on growth inhibition and apoptosis upon inhibition of either ERK or Ca^{2+} signaling are very similar.

Cell adhesion is an integral part of the complex and dynamic process of migration. Enhanced adhesion could ultimately result in both increased and decreased migration, and the context determines whether it is oncogenic or tumor suppressive. Enhanced adhesion initially results in apoptosis resistance, stimulating the development of drug resistance (40). However, when cells become increasingly oncogenic due to, for example, epithelial-to-mesenchymal transition, induction of adhesion is demonstrated to be tumor suppressive (43). Increased adhesion has been described previously as a resistance mechanism in hematologic malignancies, referred to as cell-adhesion–mediated drug resistance (CAM-DR; ref. 44). EphA4, a key player in CAM-DR, was also shown to be upregulated after afatinib treatment in our data (45). Inhibition of apoptosis in NSCLC has been shown on an mRNA level to be driven by the focal adhesion pathway (40). In our data, the main kinase involved in the regulation of focal adhesions, FAK, showed altered levels of phosphorylation, which has been associated with morphologic changes and increased adhesion (30–32). In addition, the focal adhesion–associated component Paxillin showed increased tyrosine phosphorylation, indicating increased stabilization of adhesive structures.

Published OnlineFirst July 2, 2018; DOI: 10.1158/1541-7786.MCR-18-0212

From the here presented data, regulation of the cytoskeleton was oncogenic: enhanced adhesion and decreased migration initiated by afatinib treatment most likely resulted in apoptosis resistance. Reorganization of the cytoskeleton can, among others, be established by altering Ca^{2+} homeostasis, because many adhesion and cytoskeleton remodeling-related processes are regulated in a Ca^{2+}-dependent manner (46, 47). Not surprisingly, various Ca^{2+}/Calmodulin-related proteins were found to have increased expression. On the contrary, Calmodulin itself was found to be decreased. The latter is difficult to interpret, solely based on the presented data. Future research will be aimed at determining the regulation of Ca^{2+}/Calmodulin signaling during adaptive resistance.

In order to intervene with Ca^{2+} homeostasis, we cultured the cells in the presence of EGTA, a chelating agent with great affinity for Ca^{2+}, or with $LaCl_3$, an inhibitor of plasma membrane Ca^{2+} transporters. In both cases, the sensitivity to the three EGFR inhibitors tested in four different NSCLC cell lines increased, indicating that EGFR inhibition creates a strong dependency on the accessibility of extracellular Ca^{2+} and in addition implicates a role for Ca^{2+} signaling during the development of adaptive resistance. More importantly, cells treated with EGTA or $LaCl_3$ alone did not show any response, highlighting the specificity of the combinatorial treatment. Mechanistically, we suspect that under the influence of EGFR inhibition cells either increase Ca^{2+} usage and deplete their intracellular Ca^{2+} stores, or intracellular Ca^{2+} becomes inaccessible. From literature, it is known that Ca^{2+} concentrations in the cytoplasm can be influenced by RTKs, including EGFR, which modulate PIP_2/IP_3 signaling (48). Ca^{2+} oscillations in the cell have been shown to be reduced by inhibition of the EGFR (49); therefore, it is not surprising that the magnitude of extracellular Ca^{2+} availability correlated strongly with TKI sensitivity, suggesting a direct link between inhibited EGFR signaling and Ca^{2+} dependency during adaptive resistance. However, because Ca^{2+} signaling has been implicated in many processes within the cell, future research will be aimed at determining the exact role of Ca^{2+} during the observed adaptation.

When looking at the extensive added effect Ca^{2+} deprivation, two observations stand out. First, induction of apoptosis, both in the case of TKI alone and in combination with EGTA or $LaCl_3$, only occurs 24 hours after the start of the treatment. The fact that the effects induced by an EGFR inhibitor combined with Ca^{2+} deprivation follow the effects induced by the inhibitor alone is a strong indication that development of Ca^{2+} dependency functions in a TKI-dependent manner. Second, even though the addition of extracellular Ca^{2+} deprivation caused significantly increased levels of apoptosis, eradication of the cell population is still incomplete. This behavior, similar to treatment by the TKI alone, demonstrates the adaptive capabilities of cancer cells. Even in harsh circumstances, some cells are able to survive, highlighting the need for further research into adaptive resistance mechanisms to targeted therapy.

Preceding clinical research, fundamental research is necessary to find novel targets and therapeutic strategies. Although this study is limited to cell line models, the acquired data could lead to a better understanding of cellular behavior under the pressure of an already well-studied and clinically applied drug. Using a simplified disease model, our data demonstrate that cells start to modify their signaling directly upon drug exposure, revealing an interesting therapeutic window in the study and treatment of drug resistance. It shows the necessity to increasingly study the short-term and adaptive responses of cells, in contrast with long-term, acquired mechanisms. In addition, although on a fundamental level, we revealed the involvement of calcium signaling in the adaptive response of cancer cells. Calcium signaling has been implicated in cancer previously, but to our knowledge, we are the first to show a direct link between calcium signaling and adaptive resistance of cancer cells against EGFR inhibition. Several ways exist to target calcium signaling in cancer cells (50); therefore, a logical next step would be exploring the effects of specific small-molecule inhibitors combined with existing drugs targeting calcium signaling. In addition, detailed knowledge on the behavior of key players in Ca^{2+} signaling, like Calmodulin, will shed more light on the molecular mechanisms underlying the observed effects. Furthermore, findings as presented here will need to be validated in *in vivo* models in order to be translated into a clinical application.

In conclusion, this study demonstrates that TKI-sensitive NSCLC cells use reorganization of their cytoskeleton, regulated by Ca^{2+} signaling, as an adaptive resistance mechanism. Targeting Ca^{2+} signaling sensitizes the tumor cells to TKI treatment in a TKI-dependent manner, making the global approach of the Ca^{2+} depletion highly specific. Concentrating on combinational treatment as early as possible after drug exposure in a clinical setting could improve treatment efficacy by preventing any acquired resistance mechanism from arising, rather than attempting to cure it.

Disclosure of Potential Conflicts of Interest

P. van Bergen en Henegouwen reports receiving other commercial research support from LinXis BV and has ownership interest (including stock, patents, etc.) in QVQ BV. No potential conflicts of interest were disclosed by the other authors.

Authors' Contributions

Conception and design: C. Mulder, B. Kuster, P. van Bergen en Henegouwen, S. Lemeer

Development of methodology: C. Mulder, P. van Bergen en Henegouwen, S. Lemeer

Acquisition of data (provided animals, acquired and managed patients, provided facilities, etc.): C. Mulder, N. Prust, S. van Doorn, M. Reinecke

Analysis and interpretation of data (e.g., statistical analysis, biostatistics, computational analysis): C. Mulder, N. Prust, P. van Bergen en Henegouwen, S. Lemeer

Writing, review, and/or revision of the manuscript: C. Mulder, M. Reinecke, B. Kuster, P. van Bergen en Henegouwen, S. Lemeer

Administrative, technical, or material support (i.e., reporting or organizing data, constructing databases): S. Lemeer

Study supervision: S. Lemeer

Acknowledgments

S. Lemeer acknowledges support from the Netherlands Organization for Scientific Research (NWO) through a VIDI grant (project 723.013.008). This work was supported by the Roadmap Initiative Proteins@Work (project number 184.032.201), funded by the NWO.

The costs of publication of this article were defrayed in part by the payment of page charges. This article must therefore be hereby marked *advertisement* in accordance with 18 U.S.C. Section 1734 solely to indicate this fact.

Received February 28, 2018; revised April 26, 2018; accepted June 12, 2018; published first July 2, 2018.

References

1. Minguet J, Smith KH, Bramlage CP. Targeted therapies for treatment of renal cell carcinoma: recent advances and future perspectives. Cancer Chemother Pharmacol 2015;76:219–33.
2. Hirsh V. Next-generation covalent irreversible kinase inhibitors in NSCLC: focus on afatinib. BioDrugs 2015;29:167–83.
3. Ramirez M, Rajaram S, Steininger RJ, Osipchuk D, Roth MA, Morinishi LS, et al. Diverse drug-resistance mechanisms can emerge from drug-tolerant cancer persister cells. Nat Commun 2016;7:10690.
4. Ma P, Fu Y, Chen M, Jing Y, Wu J, Li K, et al. Adaptive and acquired resistance to EGFR inhibitors converge on the MAPK pathway. Theranostics 2016; 6:1232–43.
5. Tricker EM, Xu C, Uddin S, Capelletti M, Ercan D, Ogino A, et al. Combined EGFR/MEK inhibition prevents the emergence of resistance in EGFR -mutant lung cancer. Cancer Discov 2015;5:960–71.
6. Burrell RA, Swanton C. Tumour heterogeneity and the evolution of polyclonal drug resistance. Mol Oncol 2014;8:1095–111.
7. Burrell Ra, McGranahan N, Bartek J, Swanton C. The causes and consequences of genetic heterogeneity in cancer evolution. Nature 2013;501: 338–45.
8. Sharma S V, Lee DY, Li B, Quinlan MP, Takahashi F, Maheswaran S, et al. A chromatin-mediated reversible drug-tolerant state in cancer cell subpopulations. Cell 2010;141:69–80.
9. Dolly SO, Collins DC, Sundar R, Popat S, Yap TA. Advances in the development of molecularly targeted agents in non-small-cell lung cancer. Drugs 2017;77:813–27.
10. Wen F, Li Q. Treatment dilemmas of cetuximab combined with chemotherapy for metastatic colorectal cancer. World J Gastroenterol 2016;22: 5332–41.
11. Ahn MJ, Sun JM, Lee SH, Ahn JS, Park K. EGFR TKI combination with immunotherapy in non-small cell lung cancer. Expert Opin Drug Saf 2017;16:465–9.
12. Reck M, Heigener DF, Mok T, Soria JC, Rabe KF. Management of non-small-cell lung cancer: recent developments. Lancet 2013;382:709–19.
13. Hirsch FR, Varella-Garcia M, Bunn PA, Di Maria M V.Veve R, Bremnes RM, et al. Epidermal growth factor receptor in non-small-cell lung carcinomas: correlation between gene copy number and protein expression and impact on prognosis. J Clin Oncol 2003;21:3798–807.
14. Rusch V, Baselga J, Cordon-Cardo C, Orazem J, Zaman M, Hoda S, et al. Differential expression of the epidermal growth factor receptor and its ligands in primary non-small cell lung cancers and adjacent benign lung. Cancer Res 1993;53:2379–85.
15. Ruprecht B, Zecha J, Heinzlmeir S, Médard G, Lemeer S, Kuster B. Evaluation of kinase activity profiling using chemical proteomics. ACS Chem Biol 2015;10:2743–52.
16. Ruprecht B, Koch H, Medard G, Mundt M, Kuster B, Lemeer S. Comprehensive and reproducible phosphopeptide enrichment using iron immobilized metal ion affinity chromatography (Fe-IMAC) columns. Mol Cell Proteomics 2015;14:205–15.
17. Rudolph JD, de Graauw M, van de Water B, Geiger T, Sharan R. Elucidation of signaling pathways from large-scale phosphoproteomic data using protein interaction report elucidation of signaling pathways from large-scale phosphoproteomic data using protein interaction networks. Cell Syst 2016;3:585–93.
18. Fei SJ, Zhang XC, Dong S, Cheng H, Zhang YF, Huang L, et al. Targeting mTOR to overcome epidermal growth factor receptor tyrosine kinase inhibitor resistance in non-small cell lung cancer cells. PLoS One 2013;8: e69104.
19. Shetty PK, Thamake SI, Biswas S, Johansson SL, Vishwanatha JK. Reciprocal regulation of annexin A2 and EGFR with Her-2 in Her-2 negative and herceptin-resistant breast cancer. PLoS One 2012;7:e44299.
20. Yoshida T, Zhang G, Smith MA, Lopez AS, Bai Y, Li J, et al. Tyrosine phosphoproteomics identi fi es both codrivers and cotargeting strategies for T790M-Related EGFR-TKI resistance in non – small cell lung cancer. Clin Cancer Res 2014;12–8.
21. Storr SJ, Carragher NO, Frame MC, Parr T, Martin SG. The calpain system and cancer. Nat Rev Cancer 2011;11:364–74.
22. James P, Vorherr T, Krebs J, Morellij A, Castello G, Mccormickn DJ, et al. Modulation of erythrocyte Ca2+-ATPase by selective calpain cleavage of the calmodulin-binding domain. J Biol Chem 1989; 264:8289–96.
23. Alli AA, Bao HF, Liu BC, Yu L, Aldrugh S, Montgomery DS, et al. Calmodulin and CaMKII modulate ENaC activity by regulating the association of MARCKS and the cytoskeleton with the apical membrane. Am J Physiol Ren Physiol 2015;309:F456–63.
24. Liu R, Jin JP. Calponin isoforms CNN1, CNN2 and CNN3: regulators for actin cytoskeleton functions in smooth muscle and non-muscle cells. Gene 2016;585:143–53.
25. Kania A, Klein R. Mechanisms of ephrin – Eph signalling in development, physiology and disease. Nat Rev Mol Cell Biol 2016;17:240–56.
26. Saintigny P, Peng S, Zhang L, Sen B, Wistuba II, Lippman SM, et al. Global evaluation of Eph receptors and ephrins in lung adenocarcinomas identifies EphA4 as an inhibitor of cell migration and invasion. Mol Cancer Ther 2012;11:2021–33.
27. Koch H, Busto ME, Kramer K, Medard G, Kuster B. Chemical proteomics uncovers EPHA2 as a mechanism of acquired resistance to small molecule EGFR kinase inhibition. J Proteome Res 2015;14:2617–25.
28. Eguchi R, Kubo S, Takeda H, Ohta T, Tabata C, Ogawa H, et al. Deficiency of Fyn protein is prerequisite for apoptosis induced by Src family kinase inhibitors in human mesothelioma cells. Carcinogenesis 2012;33:969–75.
29. Cheng H, Liu P, Wang ZC, Zou L, Santiago S, Garbitt V, et al. SIK1 couples LKB1 to p53-dependent anoikis and suppresses metastasis. Sci Signal 2009;2:1–12.
30. Villa-Moruzzi E. Targeting of FAK Ser910 by ERK5 and PP1delta in non-stimulated and phorbol ester-stimulated cells. Biochem J 2007;408:7–18.
31. Jacamo R, Jiang X, Lunn JA, Rozengurt E. FAK phosphorylation at Ser-843 inhibits Tyr-397 phosphorylation, cell spreading and migration. J Cell Physiol 2007;210:436–44.
32. Mitra SK, Hanson DA, Schlaepfer DD. Focal adhesion kinase: in command and control of cell motility. Nat Rev Mol Cell Biol 2005;6:56–68.
33. Vicente-Manzanares M, Ma X, Adelstein RS, Horwitz AR. Non-muscle myosin II takes centre stage in cell adhesion and migration. Nat Rev Mol Cell Biol 2009;10:778–90.
34. Leung WK, Ching AK, Wong N. Phosphorylation of caldesmon by PFTAIRE1 kinase promotes actin binding and formation of stress fibers. Mol Cell Biochem 2011;350:201–6.
35. Jiang Q, Huang R, Cai S, Wang CL. Caldesmon regulates the motility of vascular smooth muscle cells by modulating the actin cytoskeleton stability. J Biomed Sci 2010;17:6.
36. Muranyi A, Zhang R, Liu F, Hirano K, Ito M, Epstein HF, et al. Myotonic dystrophy protein kinase phosphorylates the myosin phosphatase targeting subunit and inhibits myosin phosphatase activity. FEBS Lett 2001;493:80–4.
37. Zhong X, Rescorla FJ. Cell surface adhesion molecules and adhesion-initiated signaling: understanding of anoikis resistance mechanisms and therapeutic opportunities. Cell Signal 2012;24:393–401.
38. Reddig PJ, Juliano RL. Clinging to life: cell to matrix adhesion and cell survival. Cancer Metastasis Rev 2005;24:425–39.
39. Tsai FC, Kuo GH, Chang SW, Tsai PJ. Ca2+ signaling in cytoskeletal reorganization, cell migration, and cancer metastasis. Biomed Res Int 2015;2015:409245.
40. Hsu M, Tseng C, Chen F, Hsu JT. Non-small-cell lung cancer cells combat epidermal growth factor receptor tyrosine kinase inhibition through immediate adhesion-related responses. Onco Targets Ther 2016;9: 2961–73.
41. Cargnello M, Roux PP. Activation and function of the MAPKs and their substrates, the MAPK-activated protein kinases. Microbiol Mol Biol Rev 2011;75:50–83.
42. Schwartz Ma, Assoian RK. Integrins and cell proliferation: regulation of cyclin-dependent kinases via cytoplasmic signaling pathways. J Cell Sci 2001;114:2553–60.
43. Suda K, Tomizawa K, Fujii M, Murakami H, Osada H, Maehara Y, et al. Epithelial to mesenchymal transition in an epidermal growth factor receptor -mutant lung cancer cell line with acquired resistance to erlotinib. J Thorac Oncol 2011;6:1152–61.
44. Hazlehurst LA, Dalton WS. Mechanisms associated with cell adhesion mediated drug resistance (CAM-DR) in hematopoietic malignancies. Cancer Metastasis Rev 2001;20:43–50.
45. Ding L, Shen Y, Ni J, Ou Y, Ou Y, Liu H. EphA4 promotes cell proliferation and cell adhesion – mediated drug resistance via the AKT pathway in multiple myeloma. Tumor Biol 2017;39:1010428317694298.

Published OnlineFirst July 2, 2018; DOI: 10.1158/1541-7786.MCR-18-0212

46. Giannone G, Rondé P, Gaire M, Beaudouin J, Haiech J, Ellenberg J, et al. Calcium rises locally trigger focal adhesion disassembly and enhance residency of focal adhesion kinase at focal adhesions. J Biol Chem 2004; 279:28715–23.
47. Tsai FC, Seki A, Yang HW, Hayer A, Carrasco S, Malmersjö S, et al. A polarized Ca2+, diacylglycerol and STIM1 signalling system regulates directed cell migration. Nat Cell Biol 2014;16:133–44.
48. Clapham DE. Calcium signaling. Cell 2007;131:1047–58.
49. Bryant JA, Finn RS, Slamon DJ, Cloughesy TF, Charles AC. EGF activates intracellular and intercellular calcium signaling by distinct pathways in tumor cells. Cancer Biol Ther 2004;3:1243–9.
50. Cui C, Merritt R, Fu L, Pan Z. Targeting calcium signaling in cancer therapy. Acta Pharm Sin B 2017;7:3–17.
51. Wang Y, Yang F, Gritsenko MA, Wang Y, Clauss T, Liu T, et al. Reversed-phase chromatography with multiple fraction concatenation strategy for proteome profiling of human MCF10A cells. Proteomics 2011;11:2019–26.

Published OnlineFirst July 2, 2018; DOI: 10.1158/1541-7786.MCR-18-0212

Molecular Cancer Research

Adaptive Resistance to EGFR-Targeted Therapy by Calcium Signaling in NSCLC Cells

Celine Mulder, Nadine Prust, Sander van Doorn, et al.

Mol Cancer Res 2018;16:1773-1784. Published OnlineFirst July 2, 2018.